Paper presented at the Third Turbulent Shear Flows Conference UC Davis
September 9-11, 1981

ENTRAINMENT DIAGRAMS FOR VISCOUS FLOWS

By
Brian Cantwell and Gary Allen
Department of Aeronautics and Astronautics
Stanford University
Stanford, CA 94305

ABSTRACT

A technique is described for visualizing unsteady flows which are self similar in time. The method makes use of a reduction of the equations for unsteady particle paths to an autonomous system in similarity coordinates. The entrainment diagram for a given flow corresponds to the phase portrait of this system and the flow structure is analyzed in terms of its critical points. This approach provides a powerful method for analyzing the dependence of the flow on various governing parameters.

NOMENCLATURE

a,b,c,d - matrix coefficients
f,g - self similar Falkner-Skan stream functions
G - self similar round jet stream function
H - self similar vortex ring stream function
M - governing parameter
p,q - trace and determinant of the matrix of coefficients
Re - Reynolds number
t - time
$\mathbf{u}$ - velocity vector
U_e - free stream velocity
U_o - plate velocity
x_i - spatial coordinates
β - pressure gradient exponent
ξ,η - similarity coordinates
ξ_c,η_c - coordinates of a critical point
θ - polar angle
ξ_c,θ_c - coordinates of a critical point in spherical coordinates
ω - vorticity
τ - $\ln t$

INTRODUCTION

This paper is addressed to the problem of visualizing unsteady fluid motion. Observations of organized structure in turbulence have led to an increased emphasis on direct analysis or measurement of complex unsteady flow fields. An extremely important element in current research is a renewed emphasis on the use of flow visualization and a widespread awareness that flow visualization can play a very broad role in improving our physical understanding of complicated turbulent phenomena (Kline 1978).

The instantaneous streamline patterns which result from these investigations provide a form of flow visualization combined with substantial amounts of quantitative information about the flow. However, there are significant conceptual problems involved in interpreting unsteady streamline patterns as they relate to entrainment. In an unsteady flow, streamlines can move across fluid pathlines; thus the unsteady stream function provides little insight into the behavior of the fluid itself.

Particle trajectories drawn in physical coordinates also present similar conceptual difficulties. If the integration of the particle-path equations is carried out over a volume of particles, then each point in space will be traversed by an infinite set of trajectories, each with a different slope corresponding to the passage of particles through the point at successive instants of time. In addition, the pattern of particle paths, like the pattern of streamlines, depends on the frame of reference.

Certain time-dependent flows can be reduced to a self-similar form. Such flows usually depend on one or two global parameters. In this case, some of the above objections can be removed by reducing the equations for unsteady particle paths

$$\frac{dx_i}{dt} = u_i(\underline{x},t) \qquad (1)$$

to an autonomous system in similarity coordinates. We shall call the phase portrait of this system, the entrainment diagram of the flow. It is a Lagrangian representation of the unsteady flow pattern in a system of scaled spatial coordinates. There are several useful elements of this technique

i) The entrainment diagram provides a visual picture of the flow which is invariant for various moving observers.
ii) The flow structure is described in terms of a limited set of critical points in the entrainment diagram. Thus the technique provides a quantitative scheme for identifying and classifying related features of various classes of self-similar flows.
iii) The entrainment diagram can be used to analyze the dependence of a flow on various governing parameters.

At this point it may be noted that the restriction to flows which are self-similar in time turns out to be remarkably general. Even when we further restrict ourselves to flows which are amenable to

Paper presented at the Third Turbulent Shear Flows Conference UC Davis
September 9-11, 1981

simple stretching transformations[1] the list of cases is quite long and includes virtually all of the flows which we ordinarily think of as self similar in space (Cantwell 1981).

In the present paper we will focus our attention on element (iii) of the entrainment diagram technique and demonstrate its application to the analysis of three flow problems; the classification of Falkner-Skan boundary layers, transition in the axisymmetric jet and reverse transition of the vortex ring. In each case the dependence of the flow pattern on governing parameters will be demonstrated.

EXAMPLE 1.
CLASSIFICATION OF FALKNER-SKAN BOUNDARY LAYERS

These are steady boundary layers with an imposed streamwise pressure gradient which varies according to a power law in the x-direction. Nevertheless we will begin the analysis with a similarity form appropriate to the unsteady boundary layer equations. In terms of the stream function

$$\frac{\partial^2\psi}{\partial y\partial t} + \frac{\partial\psi}{\partial y}\frac{\partial^2\psi}{\partial x\partial y} - \frac{\partial\psi}{\partial x}\frac{\partial^2\psi}{\partial y^2} = U_e\frac{\partial U_e}{\partial x} + \nu\frac{\partial^3\psi}{\partial y^3} \quad (2)$$

where the free stream velocity U_e is given by

$$U_e(x) = Mx^{\beta} \quad (3)$$

The constant, M, determines the rate at which U_e varies and is the parameter which governs the motion in the x-direction. The appropriate similarity form is

$$\psi = \nu^{1/2} M^{\frac{1}{1-\beta}} t^{\frac{1+\beta}{2(1-\beta)}} g(\xi,\eta) \quad (4)$$

where

$$\xi = \frac{x}{M^{1/(1-\beta)} t^{1/(1-\beta)}};\ \eta = \frac{y}{\sqrt{\nu t}} \quad (5)$$

Substituting (3), (4) and (5) into (2) leads to

$$\frac{1+\beta}{2(1-\beta)}\frac{\partial g}{\partial\eta} - \frac{\partial}{\partial\eta}\left[\frac{\xi}{(1-\beta)}\frac{\partial g}{\partial\xi} + \frac{\eta}{2}\frac{\partial g}{\partial\eta}\right] + \frac{\partial g}{\partial\eta}\frac{\partial^2 g}{\partial\xi\partial\eta} - \frac{\partial g}{\partial\xi}\frac{\partial^2 g}{\partial\eta 2} = \beta\,\xi^{2\beta-1} + \frac{\partial^3 g}{\partial\eta^3} \quad (6)$$

The governing partial differential equation no longer depends on time and thus (4) and (5) are correct forms. When expressed in terms of ξ and η the equations for unsteady particle trajectories become

$$\frac{d\xi}{d\tau} = g_\eta - \frac{\xi}{1-\beta} \quad (7)$$

$$\frac{d\eta}{d\tau} = -g_\xi - \frac{\eta}{2} \quad (8)$$

where $\tau = \ell n\ t$.

The Falkner-Skan solutions are usually expressed in the form

$$\psi = \left(\nu M x^{\beta+1}\right)^{1/2} f\left(y\left(\frac{M}{\nu x^{1-\beta}}\right)^{1/2}\right) \quad (9)$$

One can easily verify that (9) is equivalent to (4) where

$$g(\xi,\eta) = \xi^{(1+\beta)/2} f(s) \quad (10)$$

and $s = \eta/\xi^{(1-\beta)/2}$.

In terms of f(s) the equations (7) and (8) become

$$\frac{d\xi}{d\tau} = \xi^{\beta} f' - \frac{\xi}{1-\beta} \equiv F_1(\xi,\eta) \quad (11)$$

$$\frac{d\eta}{d\tau} = -\xi^{-\left(\frac{1-\beta}{2}\right)}\left[\frac{1+\beta}{2} f - \frac{(1-\beta)}{2} sf'\right] - \frac{\eta}{2} \equiv F_2(\xi,\eta) \quad (12)$$

In the neighborhood of a critical point (ξ_c,η_c), the above equations may be expanded as

$$\frac{d\xi}{d\tau} = a(\xi-\xi_c) + b(\eta-\eta_c) \quad (13)$$

$$\frac{d\eta}{d\tau} = c(\xi-\xi_c) + d(\eta-\eta_c) \quad (14)$$

where

$$a = \left.\frac{\partial F_1}{\partial\xi}\right|_{\xi_c,\eta_c},\ b = \left.\frac{\partial F_1}{\partial\eta}\right|_{\xi_c,\eta_c},\ c = \left.\frac{\partial F_2}{\partial\xi}\right|_{\xi_c,\eta_c},\ d = \left.\frac{\partial F_2}{\partial\eta}\right|_{\xi_c,\eta_c} \quad (15)$$

The nature of the critical point is completely determined by the trace and determinant of the matrix of coefficients.

$$p = -(a+d) \quad (16)$$

$$q = ad - bc \quad (17)$$

In order to evaluate p and q we make use of the following relations derived from setting (11) and (12) equal to zero at (ξ_c,η_c). Note $s_c = \eta_c/\xi_c^{(1-\beta)/2}$.

$$f'(s_c) = \frac{\xi_c^{1-\beta}}{1-\beta} \quad (18)$$

$$f(s_c) = 0 \quad (19)$$

Using (15), (18) and (19) the coefficients become

$$a = -1 - \left(\frac{1-\beta}{2}\right)\eta_c\xi_c^{3(\beta-1)/2} f''(s_c) \quad (20)$$

$$b = \xi_c^{3\beta/2-\frac{1}{2}} f''(s_c) \quad (21)$$

$$c = -\left(\frac{1-\beta}{2}\right)\frac{\eta_c\xi_c}{2} + \frac{\beta}{2}\frac{\eta_c}{\xi_c} - \left(\frac{1-\beta}{2}\right)^2\frac{\eta_c^2}{\xi_c}\xi_c^{\frac{3}{2}\beta-\frac{3}{2}} f''(s_c) \quad (22)$$

$$d = -\frac{(1+\beta)}{2(1-\beta)} + \frac{(1-\beta)}{2}\eta_c\xi_c^{3\beta/2-3/2} f''(s_c) \quad (23)$$

Evaluating p and q we have

$$p = -\frac{(\beta-3)}{2(1-\beta)} \quad (24)$$

[1] In the general case in two-dimensions the basic similarity variables are of the form (Cantwell 1978)
$\xi = t^{-k}\,(x-\bar{X}(t))\cos(a\ell nt + bt) - (y-\bar{Y}(t))\sin(a\ell nt + bt)$
$\eta = t^{-k}\,(x-\bar{X}(t))\sin(a\ell nt + bt) + (y-\bar{Y}(t))\cos(a\ell nt + bt)$
Where k, a and b are arbitrary constants and $\bar{X}(t)$ and $\bar{Y}(t)$ are arbitrary functions of time. In the case of simple stretching transformations $a=b=\bar{X}(t)=\bar{Y}(t)=0$.

$$q = \frac{1+\beta}{2(1-\beta)} \qquad (25)$$

Note that the evaluation of p and q does not require an explicit knowledge of f(s). Figure 1. indicates the various critical points associated with different values of β.

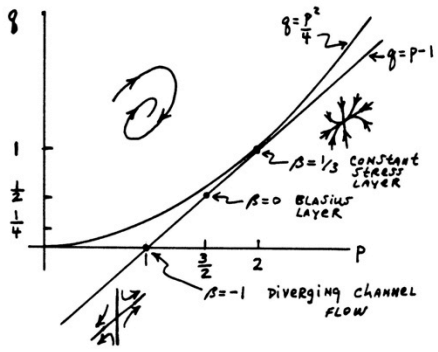

Figure 1. Trajectory of the critical point of the Falkner-Skan solutions in the (p,q) plane.

The line q=p-1 is gotten by eliminating β between (24) and (25). Well known cases include

i) (β=0) The Blasius Layer - the critical point in this case is a stable node with (p,q)= (3/2,1/2). The entrainment diagram for this flow is shown schematically in Figure 2.

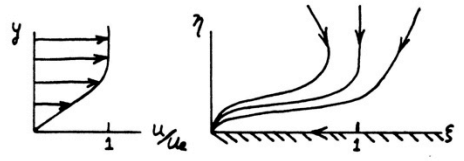

Figure 2. Entrainment diagram for the Blasius Layer.

ii) (β=1/3) Constant stress layer - this occurs where the line q=p-1 osculates with the parabola $q=p^2/4$. It represents a situation in which a mildly favorable pressure gradient balances diffusion from the wall to produce a boundary layer with a wall shear stress which remains constant with x. The entrainment diagram is similar to Figure 2. but with a star point at the leading edge.

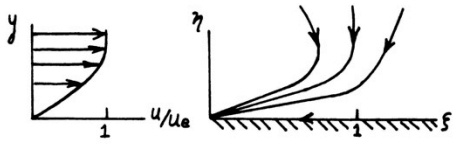

Figure 3. Entrainment diagram for the constant stress layer.

iii) (β=-1) Jeffrey - Hamel Flow - This represents the case of flow in a diverging channel produced by a volume source at the vertex. It happens to be a case where length scales in both coordinate directions vary like $\sqrt{t}$. The entrainment diagram is shown schematically in Figure 4.

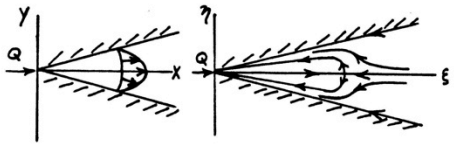

Figure 4. Entrainment diagram for the flow in a diverging channel (one possible solution).

In the context of discussing the Blasius Layer we may also consider the case of an impulsively started plate. For this case

$$u = U_o(1-\mathrm{erf}(\eta)); \quad \eta = \frac{y}{\sqrt{4\nu t}} \qquad (26)$$

The particle paths in similarity coordinates are

$$\frac{d\xi}{d\tau} = (1-\mathrm{erf}(\eta)) - \xi \qquad (27)$$

$$\frac{d\eta}{d\tau} = -\frac{\eta}{2} \qquad (28)$$

where $\xi=x/U_o t$, $n=y/\sqrt{4\nu t}$ and $\tau=\ell n\ t$.

with a critical point at $(\xi_c,\eta_c) = (1,0)$.

Near the critical point (27) and (28) may be expanded as

$$\begin{bmatrix} \frac{d\xi}{d\tau} \\ \frac{d\eta}{d\tau} \end{bmatrix} = \begin{bmatrix} -1 & 2/\sqrt{\pi} \\ 0 & -1/2 \end{bmatrix} \begin{bmatrix} \xi-1 \\ \eta \end{bmatrix} \qquad (29)$$

The critical point is a stable node with (p,q)=(3/2, 1/2); i.e. the same (p,q) values as for the steady Blasius Layer. The entrainment diagram for this flow is shown schematically in Figure 5.

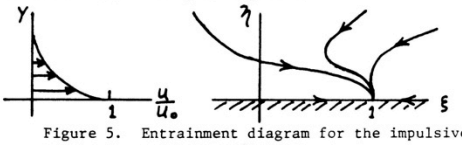

Figure 5. Entrainment diagram for the impulsively started flat plate.

Inclusion of the starting process in the analysis of the phase portrait of the particle path equations leads to a powerful method for analyzing the dynamics of fluid motion. In Example 2 we will briefly review results published previously (Cantwell 1981) for transition in the axisymmetric jet. This will serve to introduce Example 3 in which the application of the entrainment diagram technique to the problem of relaminarization or reverse transition in the impulsively produced vortex ring will be described.

The purpose for contrasting these two examples with each other is to illustrate the fundamentally different nature of the Reynolds number dependence of the two flows.

In each case we will be considering solutions of the linearized equations of motion.

$$\nabla.\bar{u} = 0 \tag{30}$$

$$\nabla x\bar{u} = \bar{\omega} \tag{31}$$

$$\frac{\partial\bar{\omega}}{\partial t} = \nu\,\nabla^2\,\bar{\omega} \tag{32}$$

EXAMPLE 2.
TRANSITION IN THE IMPULSIVELY STARTED ROUND JET

In this section we will review the behavior of an impulsively started, axisymmetric laminar jet. The Reynolds number is, $Re=(J/\rho)^{1/2}/\nu$, where J/ρ is the strength of the momentum source which produces the jet. Dimensional considerations lead to a formulation of the problem which is self similar in time in the variables $\xi = r/\sqrt{\nu t}$ and θ, where r and θ are the raduis and polar angle in spherical polar coordinates.

We will make use of the analytic solution for the limit $Re \to 0$. The Stokes stream function for this case is given by

$$\Psi = \nu^{3/2}\, t^{1/2}\, G(\xi,\theta) \tag{33}$$

Substituting (33) into (30) to (32) and solving for G leads to

$$G(\xi,\theta)= \frac{Re^2}{16\pi}\sin^2\theta\left(2\xi - \frac{4}{\sqrt{\pi}}\,e^{-\xi^2/4} - \left(2\xi - \frac{4}{\xi}\right)\mathrm{erf}\left(\frac{\xi}{2}\right)\right) \tag{34}$$

By any conventional measure the above solution has only a trivial dependence on Reynolds number. However an examination of particle trajectories associated with (33) and (34) reveals a remarkably complex structure. The equations for particle trajectories are given by

$$\frac{dr}{dt} = u(r,\theta,t;Re)\ ;\ \frac{d\theta}{dt} = \frac{v(r,\theta,t;Re)}{r} \tag{35}$$

where u and v are the radial and tangential velocities. In terms of similarity variables the equations become

$$\frac{d\xi}{d\tau} = U(\xi,\theta;Re) - \frac{\xi}{2}\ ;\ \frac{d\theta}{d\tau} = \frac{V(\xi,\theta;Re)}{\xi} \tag{36}$$

Where

$$U(\xi,\theta;Re) = \frac{1}{\xi^2\sin\theta}\frac{\partial G}{\partial\theta}\ ;\ V(\xi,\theta;Re) = \frac{-1}{\xi\sin\theta}\frac{\partial G}{\partial\xi} \tag{37}$$

and $\tau = \ln t$. Substitution of (34) into (36) using (37) leads to

$$\frac{d\xi}{d\tau} = \frac{Re^2}{2\pi}\frac{\cos\theta}{\xi^2}\left(\frac{\xi}{2} - \frac{1}{\sqrt{\pi}}\,e^{-\xi^2/4} - \left(\frac{\xi}{2} - \frac{1}{\xi}\right)\mathrm{erf}\left(\frac{\xi}{2}\right)\right) - \frac{\xi}{2} \tag{38}$$

$$\frac{d\theta}{d\tau} = -\frac{Re^2}{4\pi}\frac{\sin\theta}{\xi^2}\left(\frac{1}{2} + \frac{1}{\xi\sqrt{\pi}}\,e^{-\xi^2/4} - \left(\frac{1}{2} + \frac{1}{\xi^2}\right)\mathrm{erf}\left(\frac{\xi}{2}\right)\right) \tag{39}$$

The structure of the flow is examined by finding and classifying critical points of (38) and (39); points (ξ_c,θ_c) at which both right hand sides are equal to zero. The zeros of (39) are at ($\theta = 0,\pi$ all ξ) and ($\xi = 1.7633$ all θ) and are clearly the same for all Reynolds numbers. Setting the right hand side of (38) equal to zero gives

$$Re^2 = \frac{\pi\xi_c^3}{\left(\frac{\xi_c}{2} - \frac{1}{\sqrt{\pi}}\,e^{-\xi_c^2/4} - \left(\frac{\xi_c}{2} - \frac{1}{\xi_c}\right)\mathrm{erf}\left(\frac{\xi_c}{2}\right)\right)\cos\theta_c} \tag{40}$$

Equation (40) defines a family in the (ξ,θ) plane for various values of the Reynolds number. Intersections between (40) and the zeros of (39) locate critical points in the entrainment diagram of the solution (34). Figure 6 below shows schematically the entrainment diagram of (34) at three values of the Reynolds number.

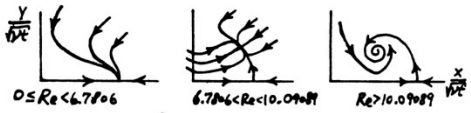

Figure 6. Entrainment diagrams of $G(\xi,\theta)$ (equation 34) for various Reynolds number ranges.

For sufficiently small Reynolds number, pathlines converge to a single stable node which lies on the axis of the jet. At a Reynolds number of 6.7806 the pattern bifurcates to a saddle lying on the axis of the jet, plus two stable nodes lying symmetrically to either side of the axis. At a Reynolds number of 10.09089 the pattern bifurcates a second time to form a saddle and two stable foci. The Reynolds number dependence of the flow is conveniently summarized by the trajectory of the critical points of (38) and (39) in the (p,q) plane shown in Figure 7.

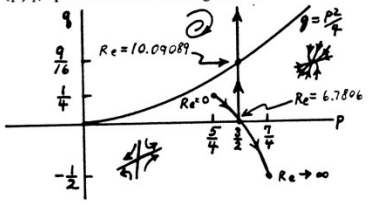

Figure 7. Trajectory of the critical points of (38) and (39) in the (p,q) plane.

Several aspects of this work which have important implications for our understanding of unsteady shear flows should be noted.

i) A vortex rollup such as that depicted in Figure 6 is usually thought of as an essentially nonlinear phenomenon. Yet here we see that a rollup process is contained in the structure of a linearized solution of the equations of motion.

ii) The vortex rollup, or focus forms just one of a family of possible critical points which may describe the structure of a given flow. In two dimensions possible critical points include saddles, nodes and foci. In three

dimensions the entrainment diagram may be very complex.

iii) One can give a physical interpretation to the three flow patterns depicted in Figure 6. Consider an interface between two fluids A and B in physical coordinates. If the momentum source is turned on at t=0 then, depending on the Reynolds number, the interface will distort into one of the three possible patterns depicted below.

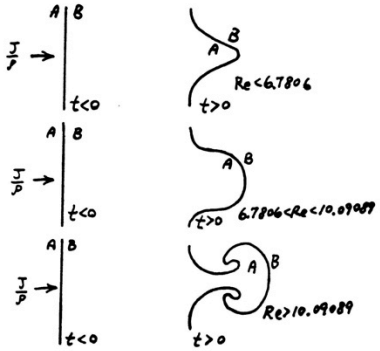

Figure 8. Distortion of fluid interface by $G(\xi,\theta)$ at three Reynolds numbers.

EXAMPLE 3.
RELAXATION OF AN IMPULSIVELY STARTED VORTEX RING

In this section we will examine the behavior of an impulsively started, axisymmetric vortex ring. The Reynolds number of the vortex ring is $Re = (I/\rho t)^{1/2}/\nu$, where I/ρ is the total impulse applied to the fluid,

$$\frac{I}{\rho} = \frac{3}{2}\int_0^{\pi}\int_0^{\infty} (u\cos\theta - v\sin\theta)2\pi r^2\sin\theta\, dr\, d\theta \qquad (41)$$

Note that, in contrast to the previous example, the Reynolds number in this flow depends on time. The equations of motion in spherical polar coordinates are

$$\frac{1}{r}\frac{\partial}{\partial r}(r^2u) + \frac{1}{\sin\theta}\frac{\partial}{\partial\theta}(v\sin\theta) = 0 \qquad (42)$$

$$r\omega = \frac{\partial}{\partial r}(rv) - \frac{\partial u}{\partial\theta} \qquad (43)$$

$$\frac{\partial}{\partial t}(r\omega) = \nu\left[\frac{1}{r^2}\frac{\partial}{\partial\theta}\left(\frac{1}{\sin\theta}\frac{\partial}{\partial\theta}(\omega\sin\theta)\right) + \frac{\partial^2}{\partial r^2}(r\omega)\right] \qquad (44)$$

with the Stokes stream function defined by

$$u = \frac{1}{r^2\sin\theta}\frac{\partial\psi}{\partial\theta}\ ;\ v = \frac{-1}{r\sin\theta}\frac{\partial\psi}{\partial r} \qquad (45)$$

As before particle paths are given by

$$\frac{dr}{dt} = u(r,\ \theta,\ t;\ \frac{I}{\rho};\ \nu) \qquad (46)$$

$$\frac{d\theta}{dt} = \frac{v(r,\ \theta,\ t;\ \frac{I}{\rho};\ \nu)}{r} \qquad (47)$$

with the parametric dependence of u and v on I/ρ and ν indicated. The variables r, θ, u and v are the same coordinates and velocities used in Example 2. The similarity forms appropriate to this problem are

$$\psi = \frac{I}{\rho}\,\nu^{-1/2}\,t^{-1/2}\,H(\xi,\theta) \qquad (48)$$

$$u = \frac{I}{\rho}\,\nu^{-3/2}\,t^{-3/2}\,U(\xi,\theta) \qquad (49)$$

$$v = \frac{I}{\rho}\,\nu^{-3/2}\,t^{-3/2}\,V(\xi,\theta) \qquad (50)$$

$$\omega = \frac{I}{\rho}\,\nu^{-2}\,t^{-2}\,W(\xi,\theta) \qquad (51)$$

$$r = \nu^{1/2}\,t^{1/2}\,\xi$$

Where U, V, H and W are the self-similar velocities, stream function and vorticity. Note that we have assumed that these functions do not depend on I/ρ or ν. We shall check this assumption a posteriori. In terms of similarity variables, the particle path equations become

$$\frac{d\xi}{d\tau} = Re^2\,U(\xi,\theta) - \frac{\xi}{2}\ ;\quad \xi = \frac{r}{\sqrt{\nu t}} \qquad (52)$$

$$\frac{d\theta}{d\tau} = Re^2\,\frac{V(\xi,\theta)}{\xi} \qquad (53)$$

where $\tau = \ln t$ and $Re^2 = I/\rho\nu^2 t$. These equations should be compared with equivalent equations for the round jet (Equations 36). Note that in this example the particle path equations do <u>not</u> reduce to an autonomous system. Rather the right hand sides of the equations depend on time, with the dependence appearing through the Reynolds number which now comes out as a parameter multiplying the as yet unknown functions $U(\xi,\theta)$ and $V(\xi,\theta)$. The entrainment diagram for this flow evolves with time.

Substituting (51) into (44) and solving the resulting equation by separation of variables leads to

$$W(\xi,\theta) = \frac{1}{16\pi^{3/2}}\sin\theta\ \xi\ e^{-\xi^2/4} \qquad (54)$$

where the constant has been chosen to insure that (41) is satisfied. The stream function is determined using (54), (45) and (43). The result is

$$H(\xi,\theta) = \frac{1}{4\pi}\sin^2\theta\left[\frac{1}{\xi}\,\mathrm{erf}\left(\frac{\xi}{2}\right) - \frac{1}{\sqrt{\pi}}\,e^{-\xi^2/4}\right] \qquad (55)$$

Taking limits gives

$$\lim_{\xi\to\infty} H(\xi,\theta) = \frac{\sin^2\theta}{4\pi\xi} \qquad (56)$$

or, in terms of ψ

$$\lim_{r\to\infty} \psi = \frac{I}{\rho}\,\frac{\sin^2\theta}{4\pi r} \qquad (57)$$

The flow at infinity is that due to a <u>steady</u> dipole of strength I/ρ. Using (45) the particle path equations become

Paper presented at the Third Turbulent Shear Flows Conference UC Davis
September 9-11, 1981

$$\frac{d\xi}{d\tau} = \frac{Re^2}{2\pi}\frac{\cos\theta}{\xi^2}\left[\frac{1}{\xi}\,\mathrm{erf}\left(\frac{\xi}{2}\right) - \frac{1}{\sqrt{\pi}}\,e^{-\xi^2/4}\right] - \frac{\xi}{2} \qquad (58)$$

$$\frac{d\theta}{d\tau} = \frac{-Re^2}{4\pi}\frac{\sin\theta}{\xi^3}\left[\frac{1}{\sqrt{\pi}}\left(1+\frac{\xi^2}{2}\right)e^{-\xi^2/4} - \frac{1}{\xi}\,\mathrm{erf}\left(\frac{\xi}{2}\right)\right] \qquad (59)$$

At this point the analysis follows very closely that used to analyze the round jet. The structure of the vortex ring is examined by finding and classifying critical points of (58) and (59); points (ξ_c,θ_c) at which both right hand sides are equal to zero. The zeros of (59) are at (θ=0, π all ξ) and (ξ=3.022437 all θ) and are clearly the same for all Reynolds numbers. Setting the right hand side of (58) equal to zero gives

$$Re^2 = \frac{\pi\xi_c^3}{\left(\frac{1}{\xi_c}\,\mathrm{erf}\left(\frac{\xi_c}{2}\right) - \frac{1}{\sqrt{\pi}}\,e^{-\xi_c^2/4}\right)\cos\theta_c} \qquad (60)$$

Intersections between (60) and the zeros of (59) locate the critical points of the system (58) and (59).

If Re < 18.174936 there is a single node lying on the axis of the vortex ring (θ_c=0). In this Reynolds number range (60) provides a relation between Re and ξ_c, the radial coordinate of the node which moves outward along the axis of the vortex ring as Re is increased.

When Re exceeds 18.174936 the flow splits into three critical points; a saddle situated on the axis of the vortex ring and two stable nodes lying symmetrically about the axis at ξ_c=3.022437 and

$$\theta_c = \pm\cos^{-1}\left[\left(\frac{18.174936}{Re}\right)^2\right] \qquad (61)$$

As the Reynolds number is further increased, the nodes move away from the axis on the circle ξ_c=3.022437. At the same time the ξ_c coordinate of the saddle continues to follow (60) with θ_c=0. For the critical point on the axis, the invariants of the matrix of coefficients are

$$p_{\theta_c=0} = \frac{3}{2} - \frac{Re^2}{4\pi\xi_c^3}\left[\frac{1}{\sqrt{\pi}}\left(1+\frac{\xi_c^2}{2}\right)e^{-\xi_c^2/4} - \frac{1}{\xi_c}\,\mathrm{erf}\left(\frac{\xi_c}{2}\right)\right] \qquad (62)$$

$$q_{\theta_c=0} = \left(p_{\theta_c=0} - \frac{3}{2}\right)\left(\frac{3}{2} - 2\,p_{\theta_c=0}\right) \qquad (63)$$

For the critical point off the axis, the invariants are (ξ_c evaluated as 3.022437)

$$p_{\theta_c\neq 0} = \frac{3}{2} \qquad (64)$$

$$q_{\theta_c\neq 0} = 2.94130154 \times 10^{-6}\;Re^4 - 3.20945389 \times 10^{-1} \qquad (65)$$

The off-axis node changes to a stable focus when $q_{\theta_c\neq 0}$ exceeds 9/16. This occurs at Re=23.410465. Figure 9 shows schematically the entrainment diagram of the vortex ring at three values of the Reynolds number

Figure 9. Entrainment diagrams of $H(\xi,\theta)$ (equation 55) for various Reynolds number ranges.

The various patterns and their limiting forms at ξ_c=0 and ξ_c=∞ (Re=0, Re=∞) are summarized in Figure 10 which shows the trajectory of the critical points of the vortex ring in the (p,q) plane.

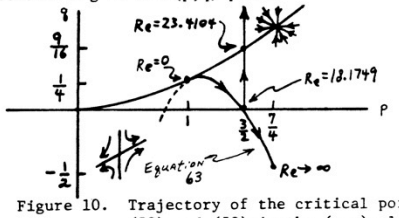

Figure 10. Trajectory of the critical points of (58) and (59) in the (p,q) plane.

Note that the trajectory is almost identical to that of the round jet (Figure 7). The main difference is in the limiting values of p and q as Re→0 (ξ_c→0). In the case of the vortex ring the (p,q) trajectory (Equation (62)) osculates with the parabola $q=p^2/4$; i.e. the on-axis critical point becomes a star (p=1, q=1/4) as Re→0. Whereas the zero Reynolds number limit in the case of the round jet was a stable node (p=5/4, q=1/4).

While the similarities between these two examples may be quite striking, the physical interpretation of the results is totally different. In the case of the round jet the pathline equations are strictly autonomous and, in a given realization of the flow the Reynolds number is constant over all space and time. In the case of the vortex ring the pathline equations are not autonomous and, in a given realization all Reynolds numbers are encountered with the Reynolds number decreasing with increasing time ($Re\sim 1/\sqrt{t}$). The appropriate mixing problem to imagine in this case is one in which a series of interfaces is encountered by a single vortex ring as shown schematically in Figure 11.

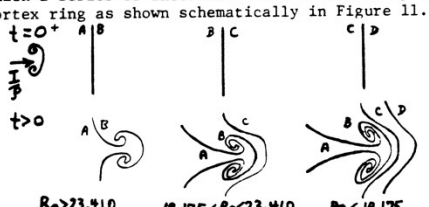

Figure 11. Mixing at several interfaces by a vortex ring.

The first interface encountered by the vortex ring rolls up in the traditional fashion. The second and third interfaces are placed sufficiently far from the origin so that the Reynolds number of the arriving ring has dropped below the appropriate threshold value. These latter two interfaces never roll-up.

ACKNOWLEDGEMENT

This work was supported by NASA Ames Research Center under NASA Grant NSG-2392.

REFERENCES

1) Kline, S.J. 1978. The Role of Visualization in the Study of the Structure of the Turbulent Boundary Layer. Lehigh Workshop on Coherent Structure of Structure of Turbulent Boundary Layers, ed. C.R. Smith, D.E. Abbott pp 1-26.

2) Cantwell, B.J. 1981[1]. Organized Motion in Turbulent Flow. Ann. Rev. Fluid Mech. 13:457-515.

3) Cantwell, B.J. 1978[2]. Similarity Transformations for the Two Dimensional Unsteady Stream Function Equation. J. Fluid Mech. 85:257-271.

4) Cantwell, B.J. 1981. Transition in the Axisymmetric Jet. J. Fluid Mech. 104:369-386.